EurJIC
European Journal of Inorganic Chemistry

Research Article
doi.org/10.1002/ejic.202101046

Chemistry Europe
European Chemical Societies Publishing

www.eurjic.org

2H1C Mimicry: Bioinspired Iron and Zinc Complexes Supported by *N,N,O* Phenolate Ligands

Emily C. Monkcom,[a] Hidde A. Negenman,[a] Eduard Masferrer-Rius,[a] Martin Lutz,[b] Shengfa Ye,[c] Eckhard Bill,[d] and Robertus J. M. Klein Gebbink*[a]

In pursuit of mimicking the ubiquitous 2H1C motif in mononuclear non-heme iron enzymes, two new bioinspired *N,N,O* phenolate ligands, **BenzImNNO** and **Im^{Ph2}NNO**, are synthesised and their coordination chemistry with zinc(II) and iron(II) is explored. **BenzImNNO** coordinates by means of an anionic κ_3-*N,N,O* donor set and readily forms homoleptic bisligated complexes, also in the presence of equimolar amounts of metal salt. In contrast, the increased steric bulk of **Im^{Ph2}NNO** promotes the formation of dinuclear complexes, $[M_2(Im^{Ph2}NNO)_2(OTf)_2]$ (M = Fe, Zn), with facially opposing metal sites, as a result of its unique bridging μ_2:κ_2-N,N:κ_1-O coordination mode. We investigate the robustness of the ligand's dinucleating coordination mode during oxidative transformations and demonstrate that its coordination mode is retained upon triflate substitution for a biorelevant thiophenolate co-ligand.

Introduction

The 2-His-1-Carboxylate facial triad (2H1C) is a bioinorganic motif that has been identified at the active site of a superfamily of mononuclear non-heme iron oxygenase and oxidase enzymes (Figure 1).[1–3] It comprises two neutral histidine (His) residues and one anionic carboxylate group, typically an aspartate (Asp) or a glutamate (Glu), that coordinate in a facial, tripodal arrangement to a single metal ion. As well as anchoring the metal site in place within the protein scaffold, the 2H1C ensures that three mutually *cis* vacant sites are available for substrate, co-substrate or dioxygen binding during catalysis. Typically, loosely bound water molecules occupy these sites in the enzyme's resting state (Figure 1). The 2H1C is so ubiquitous at the active sites of mononuclear O_2-activating non-heme iron enzymes that it can be regarded as an entity almost independent of any host protein scaffold and is currently regarded as one of the most versatile structural motifs with which nature carries out oxidative transformations. The 2H1C has served as a founding architectural model for a wide variety of bioinspired ligands, developed by the bioinorganic community to synthetically model enzyme active sites and better understand the mechanistic pathways underlying enzyme function.[4–7] Over the years, many efforts have been made towards the development of so-called *"N,N,O* ligands", designed to model the structural aspects of the 2H1C as faithfully as possible by incorporating two N-donors and an O-donor within

[a] *E. C. Monkcom, H. A. Negenman, E. Masferrer-Rius, Prof. Dr. R. J. M. Klein Gebbink*
Organic Chemistry and Catalysis,
Debye Institute for Nanomaterials Science,
Utrecht University,
Universiteitsweg 99, 3584 CG,
Utrecht, The Netherlands
E-mail: r.j.m.kleingebbink@uu.nl
www.uu.nl/en/research/organic-chemistry-catalysis
[b] *Dr. M. Lutz*
Structural Biochemistry,
Bijvoet Centre for Biomolecular Research,
Utrecht University,
Universiteitsweg 99, 3584 CG,
Utrecht, The Netherlands
[c] *Prof. Dr. S. Ye*
State Key Laboratory of Catalysis,
Dalian Institute of Chemical Physics,
Chinese Academy of Sciences,
457 Zhongshan Road, Dalian
116023, China
[d] *Dr. E. Bill*
Max-Planck-Institut für Chemische Energiekonversion,
Kaiser-Wilhelm-Platz 1, 45470
Mülheim an der Ruhr, Germany

Supporting information for this article is available on the WWW under https://doi.org/10.1002/ejic.202101046

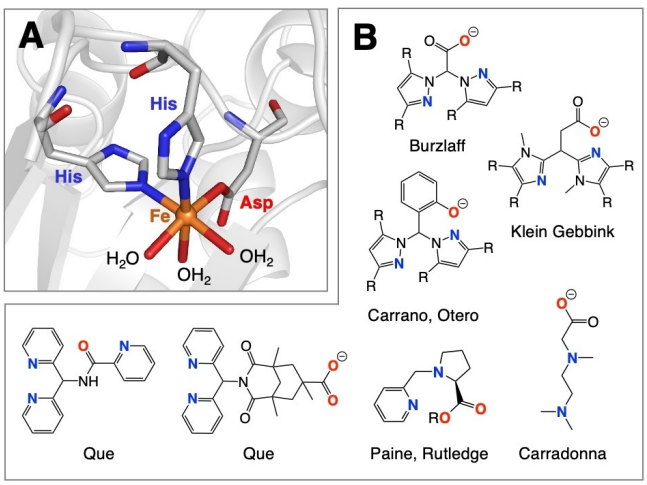

Figure 1. A: The 2-His-1-Carboxylate facial triad (2H1C) at the active site of deacetoxycephalosporin C synthase (DAOCS, PDB 1RXF).[21] B: Selected examples of *N,N,O* ligand designs.

Research Article
doi.org/10.1002/ejic.202101046

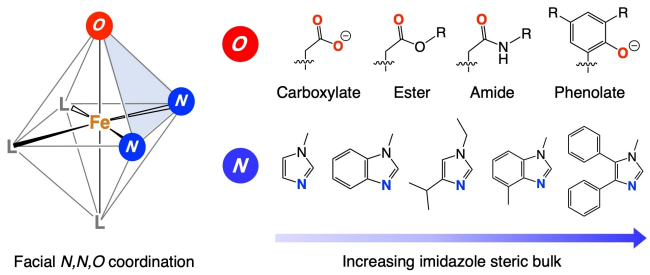

Figure 2. The variation in bis-imidazole-derived *N,N,O* ligands.

a facial, tridentate coordination motif (Figure 1). However, obtaining mononuclear, monoligated iron complexes with such ligands is challenging due to their low denticity as well as the inherent ligand lability exhibited by high-spin iron centres. Notable examples of *N,N,O* ligands include the bis-pyrazolyl acetate ligand family developed in the group of Burzlaff,[8–11] the bis-pyrazolyl phenolate ligand family developed by the groups of Carrano and Otero,[12–14] the carboxylate-tethered ethylenediamine ligands reported by Caradonna and co-workers,[15,16] the amide- or carboxylate-tethered bis-pyridyl ligands developed in the group of Que,[17,18] and the L-proline-derived ligands reported by the groups of, amongst others, Paine and Rutledge.[19,20]

Our group has focused on the development of bis-imidazole derived *N,N,O* ligands, since imidazoles are of particular biorelevance to the histidyl imidazole side-chain found in enzymatic systems.[22–27] Our studies show that achieving monoligated, *N,N,O*-bound iron complexes is highly dependent on the steric bulk of the imidazole groups as well as the nature of the O-donor (Figure 2).[28] While anionic carboxylates are the most biologically relevant O-donor, these have the tendency to engage in bridging coordination modes that can disrupt the ligand's *N,N,O* coordination and lead to the formation of coordination oligomers.[23] Esters and amides, on the other hand, have the advantage that their solubility and steric properties can easily be tuned by varying the nature of their tethered organic substituent.[24,26] However, the neutral charge of these O-donors deviates somewhat from the electronic properties of the 2H1C and is associated to a greater degree of coordination lability.[27]

Phenolates are an attractive means with which to incorporate an anionic O-donor into the *N,N,O* ligand design that can be tuned both sterically and electronically. However, phenolates can also engage in mono- or dinucleating (bridging) coordination modes, due to the availability of two lone pairs on the anionic oxygen atom.[29] Control of this nuclearity is typically dependent on the size and positioning of substituents on the phenolate ring. Previously, our group demonstrated that bis-imidazole-derived phenolate ligand **ImNNO** (Figure 3) can coordinate facially to an iron centre by means of its *N,N,O* donor set.[30] However, the small size of its constituent donor groups enables two ligand molecules to bind simultaneously to an iron(III) centre, producing a homoleptic, bisligated complex, $[Fe(ImNNO)_2]^+$. A monoligated iron complex was successfully synthesised by including one equivalent of tetrachlorocatecholate (tcc) as an exogenous co-ligand, which could block the coordination of a second ligand equivalent. More recently, we reported the synthesis of mononuclear iron and zinc complexes supported by ligand **Im^{Ph2}NNO^{tBu}**, which features bulky substituents on all of its donor groups, including *tert*-butyl groups on the phenolate ring and phenyl groups on the imidazole heterocycles.[31]

In order to investigate the influence of the substituents on the phenol donor moiety in this ligand class, we have synthesised two new bis-imidazole-derived phenolate ligands, **BenzImNNO** and **Im^{Ph2}NNO**, which incorporate unsubstituted phenolate moieties and either 1-methyl-*1H*-benzimidazole or 1-methyl-4,5-diphenyl-*1H*-imidazole heterocycles, respectively. In this study, we report on the development of these ligands and investigate their coordination chemistry in solution and the solid state towards both iron(II) and zinc(II). The electronic and magnetic properties of the resulting mono- and dinuclear iron complexes are investigated by means of Mössbauer spectroscopy and SQUID magnetometry. Finally, we examine the robustness of the ligand coordination modes during oxidative transformations and ligand exchange studies involving a thiophenolate co-ligand.

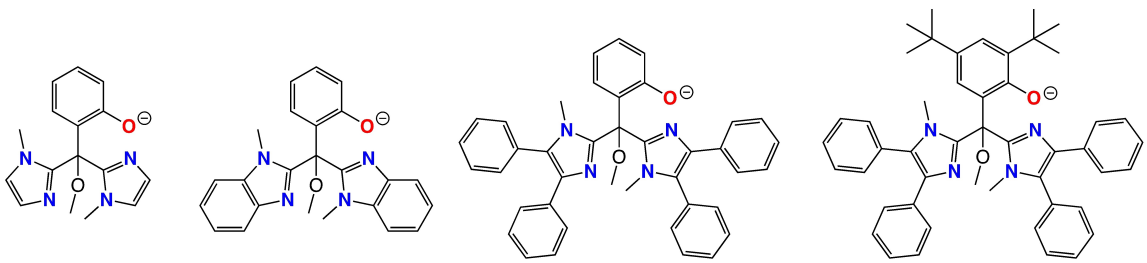

Figure 3. Bis-imidazole phenolate ligands with an *N,N,O* donor set.

Research Article
doi.org/10.1002/ejic.202101046

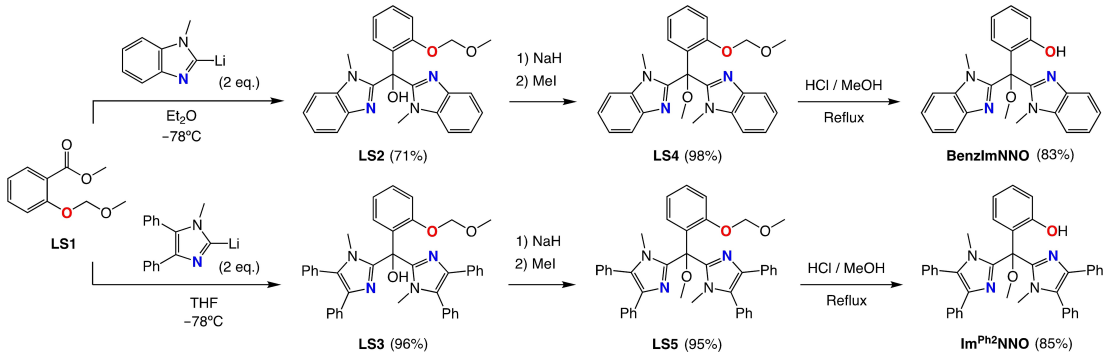

Scheme 1. Synthesis of **H-BenzImNNO** and **H-Im^{Ph2}NNO**.

Results and Discussion

Ligand synthesis and characterisation

The ligands **H-BenzImNNO** and **H-Im^{Ph2}NNO** can be readily synthesized on a multigram scale, using a procedure adapted from Jameson *et al.*[32] that incorporates 1-methyl-*1H*-benzimidazole or 1-methyl-4,5-diphenyl-*1H*-imidazole into the ligand designs, respectively (Scheme 1). The synthesis begins with the methylmethoxy ether (MOM) protection of methyl salicylate, affording **LS1** in 89% yield. Next, two equivalents of the desired imidazole are deprotonated with *n*-BuLi, and the resulting lithium imidazolium salt is reacted with **LS1**. For 1-methylbenzimidazole, it is essential to perform this step in anhydrous diethyl ether in order to generate **LS2** cleanly in 71% yield. For 1-methyl-4,5-diphenylimidazole, this reaction proceeds cleanly in anhydrous THF, affording **LS3** in 96% yield. Due to their sterically encumbered nature, the subsequent methylation of **LS2** and **LS3** is kinetically slow and requires a large excess of NaH and MeI as well as overnight stirring to form **LS4** and **LS5** in 98% and 95% yields, respectively. Protection of the tertiary alcohol in this manner prevents any ambiguity in the potential donor set of the ligand. Finally, the MOM-group is cleaved under acidic conditions, affording the phenols **H-BenzImNNO** and **H-Im^{Ph2}NNO** in 83% and 85% yield, respectively.

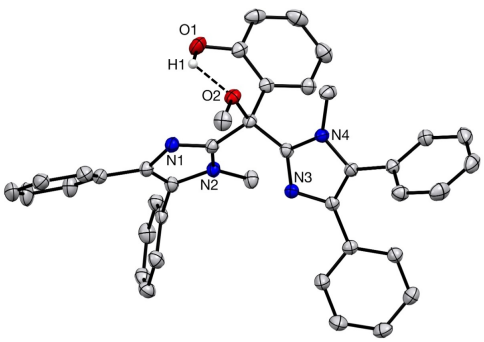

Figure 4. Displacement ellipsoid plot (50% probability level) for **H-Im^{Ph2}NNO** in the solid state. All C–H hydrogen atoms have been omitted for clarity. The intramolecular hydrogen bond is depicted with a dashed line.

In ^{1}H NMR spectroscopy, the phenolic protons in **H-BenzImNNO** and **H-Im^{Ph2}NNO** manifest themselves as broad singlets at 10.36 and 10.35 ppm, respectively. For both ligands, a relatively sharp O-H vibration is also observed at approximately 3390 cm^{-1} by solid-state IR spectroscopy. **H-Im^{Ph2}NNO** crystallises overnight as small colourless blocks from the slow vapour diffusion of hexane into a THF solution of the compound at room temperature. The X-ray crystal structure confirms the structure of **H-Im^{Ph2}NNO** and reveals the presence of an intramolecular hydrogen bond between the methoxy group and the phenolic proton, analogous to that observed by Bruijnincx *et al.* for **H-ImNNO**,[28] which orientates the phenol away from the potential metal coordination site (Figure 4). From this, it can already be deduced that deprotonation of this ligand precursor to its phenolate form could promote the facial, anionic *N,N,O* coordination of this bulky ligand scaffold by eliminating the H-bonding interaction and creating a more strongly donating phenolate O-donor.

Coordination chemistry of BenzImNNO with $ZnCl_2$

H-BenzImNNO was dissolved in THF and deprotonated using a slight excess of KH. After stirring for 1 h, the bright yellow solution was filtered and one equivalent of $ZnCl_2$, suspended in THF, was added to the mixture. The reaction was stirred for another 3 h, after which the solvent was removed under vacuum. The residual brown solid was extracted with MeCN, the solution filtered, and the solvent removed under vacuum. The resulting complex, [Zn(BenzImNNO)$_2$ZnCl$_2$] (**1**), was obtained in 54% yield (Scheme 2). The X-ray crystal structure of **1** (Figure 5)[28] reveals that it is a dinuclear complex. The first zinc ion (Zn1) has a distorted octahedral geometry, facially capped by the anionic κ_3-*N,N,O* donor set of two **BenzImNNO** molecules. The second zinc ion (Zn2) has a distorted tetrahedral geometry, coordinated by two chloride ions and the μ_2-bridging phenolic oxygen atoms of both ligand molecules. The zinc centres are comprised within a Zn_2O_2 diamond core and are separated by an intermetallic distance of 3.1162(8) Å. The longer Zn1–O and shorter Zn2–O distances reflect the more electron-rich and poor natures of the octahedral and tetrahedral

Research Article
doi.org/10.1002/ejic.202101046

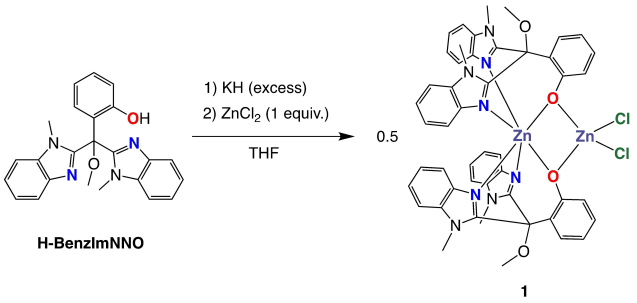

Scheme 2. Synthesis of $[Zn(BenzImNNO)_2ZnCl_2]$ (**1**).

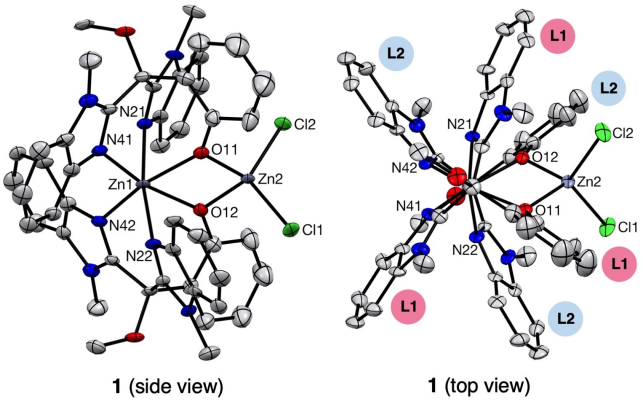

Figure 5. Displacement ellipsoid plot (50% probability level) for **1** in the solid state.[28] All H atoms have been omitted for clarity. L1 and L2 indicate the phenolate and imidazole groups belonging to two different ligand molecules.

zinc ions, respectively. In both cases, the Zn–O bond lengths are slightly longer than those typically reported for mononuclear zinc complexes of similar geometries, which we attribute to the bridging coordination mode of the phenolate.

This structure demonstrates that the reaction between equimolar amounts of **BenzImNNO** and $ZnCl_2$ does not produce a mononuclear, monoligated complex. Instead, the κ_3-*N,N,O* coordination of two ligand molecules to one zinc ion appears to be thermodynamically favoured, generating a homoleptic, bisligated complex to which the remaining equivalent of $ZnCl_2$ coordinates *via* the distal lone pairs of the phenolic O-donors. The co-ligation of $ZnCl_2$ in this manner causes the phenolic O-donors to orientate themselves *cis* to each other, which results in the staggered arrangement of both ligand molecules about Zn1. This gives the complex a "butterfly" structure in its solid state (Figure 5, top view). A similar dinuclear nickel(II) complex was reported by Higgs *et al.* employing a tripodal *N,N,O* bis-3,5-dimethyl-pyrazolyl-derived phenolate ligand.[12] The "butterfly" structure of **1** effectively gives rise to two distinct chemical environments for the benzimidazole groups of each **BenzImNNO** ligand molecule (i.e. they are magnetically inequivalent). This is in line with the solution-state structure of **1** observed by ^{1}H NMR spectroscopy (Figure 6), where three distinct singlets are observed at 4.34, 3.79 and 3.49 ppm with a 1:1:1 relative integral ratio that correspond to the two N-methyl groups and

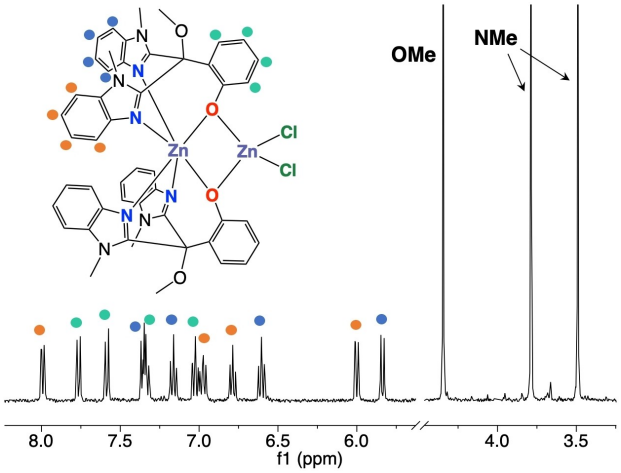

Figure 6. ^{1}H NMR (400 MHz) spectrum of **1**, recorded in CD_2Cl_2 at 25 °C.

the O-methyl group of the **BenzImNNO** ligand scaffold. Similarly, 12 different aromatic multiplets are observed, each with a relative integration of 1H, which corresponds to the 8 hydrogens of the benzimidazole rings and the 4 hydrogens of the phenolate ring per ligand molecule.

Coordination chemistry of BenzImNNO with $Zn(OTf)_2$

Next, we investigated the coordination chemistry of **BenzImNNO** with $Zn(OTf)_2$ in order to examine the effect of potentially non-coordinating triflate anions. Analogously to the preparation of **1**, **H-BenzImNNO** was dissolved in THF and deprotonated using a slight excess of KH. The resulting bright yellow phenolate solution was filtered and one equivalent of $Zn(OTf)_2$ in THF was added dropwise to the filtrate (Scheme 3). The resulting mixture was stirred for a further 3 h, after which the solvent was removed under vacuum. The residual solid was extracted into CH_2Cl_2 solution, filtered and dried, affording $[Zn(BenzImNNO)_2Zn(OTf)_2]$ (**2**) as a pale yellow solid in 72% yield.

The ^{1}H NMR spectrum of the **2** recorded in acetonitrile-d_3 at 25 °C is shown in Figure 7 (middle). In the aliphatic region of the spectrum, we observe a sharp singlet at 3.47 ppm and a

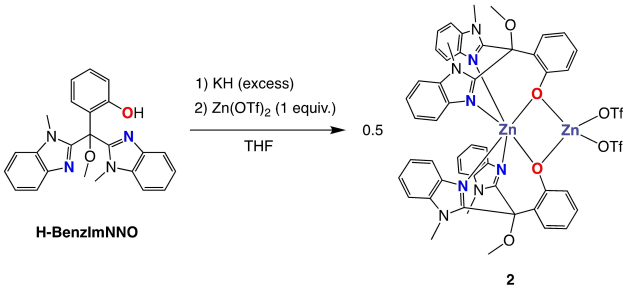

Scheme 3. Synthesis of $[Zn(BenzImNNO)_2Zn(OTf)_2]$ (**2**). The structure of **2** is proposed on the basis of NMR analysis.

Research Article
doi.org/10.1002/ejic.202101046

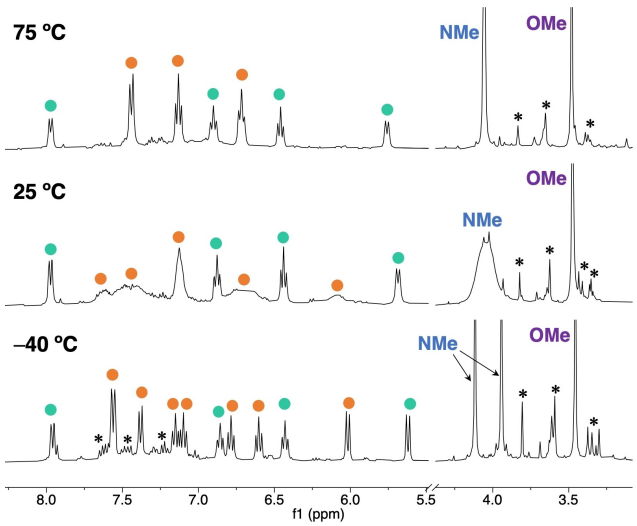

Figure 7. Variable temperature ^{1}H NMR (400 MHz) spectra of **2**, recorded in CD_3CN. Unknown impurities are denoted with a black asterisk. Signals associated to the **BenzImNNO** benzimidazole and phenolate rings are highlighted with orange and green labels, respectively.

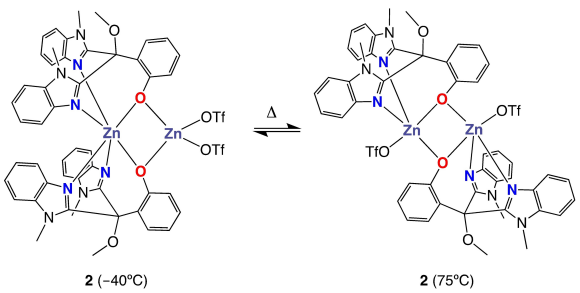

Scheme 4. Fluxional behaviour of [Zn(BenzImNNO)$_2$Zn(OTf)$_2$] (**2**).

broad signal at 4.04 ppm, which, on the basis of their 1:2 relative integral ratio, are assigned to the O- and N-methyl groups, respectively. In the aromatic region of the spectrum, four well-resolved multiplets are detected at 7.98, 6.88, 6.44 and 5.70 ppm, all of which integrate to 1H relative to the O-methyl signal.

By means of 1D total correlation spectroscopy (TOCSY) (Figures S38), we assign these signals to the aromatic hydrogens of the **BenzImNNO** phenolate ring. Other much broader aromatic signals are also observed, whose combined integration totals approximately 8H. We tentatively assign these to the aromatic hydrogens of the benzimidazole rings. The severe broadening of the signals associated to the benzimidazole groups indicates that these are highly fluxional in acetonitrile solution. Similar broadening of the NMR signals is also observed in dichloromethane-d_2 (Figure S36), so we exclude solvent coordination as being the cause of this fluxional behaviour. We investigated the fluxional behaviour of the complex by means of variable temperature (VT) NMR analysis (Figure 7).

Cooling the sample to -40 °C causes the broad N-methyl resonance to split into two sharp singlets at 4.12 and 3.94 ppm with a relative integral ratio of 1:1. Similarly, the broad aromatic signals sharpen and produce eight new well-resolved multiplets, each of which integrates to 1H (the doublet at 7.57 ppm comprises two separate doublets that are perfectly overlapped). By means of 1D TOCSY, 1D NOE, EXSY and NOESY NMR experiments (see Figures S43-S48), we could assign all signals and we propose that **2** is analogous in structure to **1** at low temperature, involving μ_2-bridged phenolate coordination to $Zn(OTf)_2$ instead of $ZnCl_2$. Warming the sample to 75 °C causes the N-methyl benzimidazole resonance to sharpen significantly while retaining its 2:1 relative integral ratio with the O-methyl signal, consistent with C_S-symmetry of the **BenzImNNO** ligand scaffold. Similarly, the broad signals in the aromatic region of the spectrum assigned to the H-atoms at the 5-, 6- and 7-positions of the two benzimidazole rings coalesce to produce three well-resolved multiplets at 7.45, 7.13 and 6.72 ppm, each of which integrates to 2H. However, the two aromatic resonances associated to the hydrogens at the benzimidazole 4-positions broaden so significantly that they are no longer observed at high temperature. On this basis, we propose that higher temperatures provoke significant structural rearrangements of **2**, where both zinc atoms become pentacoordinate, bound to the κ_3-*N,N,O* donor set of a **BenzImNNO** ligand, a terminal triflate anion and the bridging phenolate of the second ligand molecule (Scheme 4). We attribute the high fluxionality of **2** to the weakly coordinating nature of the triflate anions, which, in contrast to **1**, causes the benzimidazole groups to easily exchange between the two zinc ions.

For comparison, **BenzImNNO** was reacted with 0.5 equiv. $Zn(OTf)_2$. Interestingly, the resulting ^{1}H NMR spectrum, displayed in Figure 8, contains two different sets of signals. The first set of signals (labelled with green circles) is identical to the NMR spectrum of **2** at 25 °C. The second set of signals (labelled with blue circles) contains two sharp resonances at 3.68 and 3.35 ppm with a relative integral ratio of 2:1, that we assign to the N- and O-methyl groups of the **BenzImNNO** ligand,

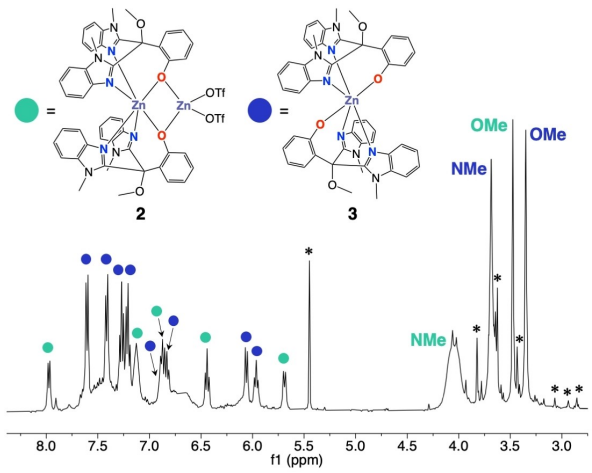

Figure 8. ^{1}H NMR spectrum (400 Hz) of the product mixture obtained from the reaction of **BenzImNNO** with 0.5 equiv. $Zn(OTf)_2$. Spectrum is recorded in CD_3CN at 25 °C. Residual solvent and unknown impurities are denoted by black asterisks.

Research Article
doi.org/10.1002/ejic.202101046

respectively. This is indicative of C_S ligand symmetry, where both benzimidazoles are chemically equivalent. In the aromatic region of the spectrum, four multiplets are observed at 7.62, 7.42, 7.27 and 7.21 ppm that each integrate to 2H, and four signals are detected at 6.90, 6.44, 6.07 and 5.96 ppm that each integrate to 1H. We assign these two sets of aromatic signals to the aromatic hydrogens of the benzimidazole and phenolate groups, respectively. The 2:1 relative integral ratio suggests C_s ligand symmetry. Given the sharp and well-resolved nature of all resonances, we hypothesise that this species has a much lower degree of fluxional behaviour in solution and likely corresponds to a homoleptic, bisligated zinc complex, [Zn-(BenzImNNO)$_2$] (**3**). Based on the integral values of the O-methyl singlets, we calculate that **2** and **3** were formed in approximately equimolar amounts. Importantly, the ^{1}H NMR signals we observe for **3** are different to those of **2** at 75 °C. On this basis, we exclude the formation of **3** when reacting **BenzImNNO** with 1 equivalent of Zn(OTf)$_2$.

Single crystals suitable for X-ray diffraction were obtained from the slow diffusion of *n*-pentane into a dichloromethane solution of the reaction product mixture. The resulting X-ray crystal structure (Figure 9) corroborates the structural hypothesis for **3**, where two **BenzImNNO** molecules coordinate facially by means of their *N,N,O* donor set to a single, octahedral zinc(II) ion. The phenolic O-donors are coordinated mutually *trans* at the axial sites of the complex, while the imidazolyl nitrogen atoms are coordinated within the equatorial plane. The zinc ion is located on an inversion centre. Due to the mononucleating coordination mode of its phenolic O-donors, the Zn–O distances in **3** are significantly shorter than the octahedral Zn–O bond distances in **1**. Selected bond lengths and bond angles are given in Table S2.

Overall, these results demonstrate that ligand **BenzImNNO** can facially cap a metal centre by means of its anionic *N,N,O* donor set. However, the ligand is small enough to allow two ligand molecules to coordinate the same metal centre and we do not observe the thermodynamic formation of mononuclear, monoligated complexes. Interestingly, the increased steric bulk of the benzimidazole groups in **BenzImNNO** compared to the imidazoles in **ImNNO** does have an impact on the coordination of the phenolic oxygen atom, promoting its coordination through the distal oxygen lone pair (e.g. in **1** and in the proposed structure of **2**) as well as the proximal lone pair (e.g. in **3**). Based on these results, we decided not to proceed with the corresponding iron(II) chemistry of **BenzImNNO** as we believe homoleptic bisligated iron complexes are likely to form. Instead, we proceeded to investigate the coordination chemistry of the bulkier **Im^{Ph2}NNO** ligand variant in the quest for monoligated *N,N,O*-bound metal complexes.

Coordination chemistry of ligand Im^{Ph2}NNO

The coordination chemistry of anionic **Im^{Ph2}NNO** was explored with both iron and zinc (Scheme 5). The ligand precursor was dissolved in THF and deprotonated using a slight excess of KH. After stirring for 1 h, the yellow ligand salt solution was filtered and an equimolar amount of iron(II) or zinc(II) triflate in THF was added dropwise to the solution. This caused a rapid colour change to orange (in the case of iron) or to pale yellow (in the case of zinc). The reaction mixtures were stirred for 1 h and were subsequently filtered and concentrated under vacuum. The residual solids were then extracted with dichloromethane and the solutions were filtered to remove the insoluble KOTf. [Fe$_2$(Im^{Ph2}NNO)$_2$(OTf)$_2$] (**4**) and [Zn$_2$(Im^{Ph2}NNO)$_2$(OTf)$_2$] (**5**) were obtained as white solids in yields of 70% and 59%, respectively. Analogous reactions involving $FeCl_2$ and $ZnCl_2$ afforded highly insoluble products, which hampered any further purification or characterisation.

Single crystals of **4** and **5** suitable for X-ray diffraction were obtained by slow vapour diffusion of *n*-hexane into THF solutions of the complexes under ambient conditions. The X-ray crystal structures (Figure 10) show that **4** and **5** are analogous in structure, each comprising two metal ions and two ligand molecules bound together in a cyclic 14-membered ring configuration. Each metal centre is tetracoordinate and has a distorted tetrahedral geometry. The **Im^{Ph2}NNO** ligands assume a bridging μ_2:κ_2-*N,N*:κ_1-*O* coordination mode, where the two imidazole N-donors bind to one metal centre and the anionic phenolate O-donor binds to the second metal centre. Although this is not a κ_3 coordination mode, each metal ion is effectively coordinated by a tripodal *N,N,O* binding motif. The fourth "apical" coordination site of each metal ion is occupied by a

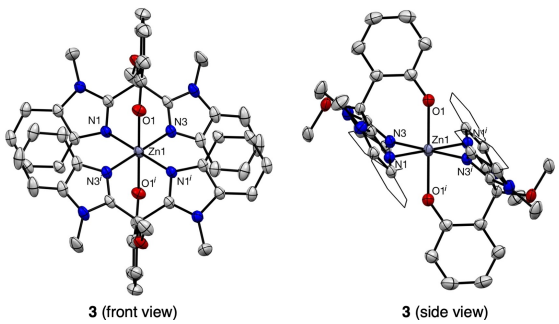

Figure 9. Displacement ellipsoid plot (50% probability level) for **3**. For the side view, the benzimidazole phenyl rings have been depicted in the wireframe format for clarity. All H-atoms and disordered solvent molecules have been omitted for clarity. Symmetry code *i*: 5/3-*x*, 4/3-*y*, 1/3-*z*.

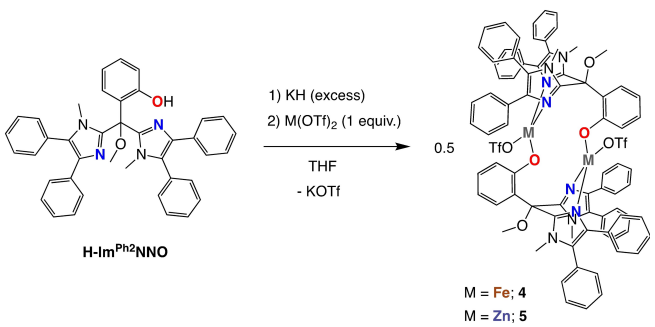

Scheme 5. The synthesis of dinuclear complexes [Fe$_2$(Im^{Ph2}NNO)$_2$(OTf)$_2$] (**4**) and [Zn$_2$(Im^{Ph2}NNO)$_2$(OTf)$_2$] (**5**).

Research Article
doi.org/10.1002/ejic.202101046

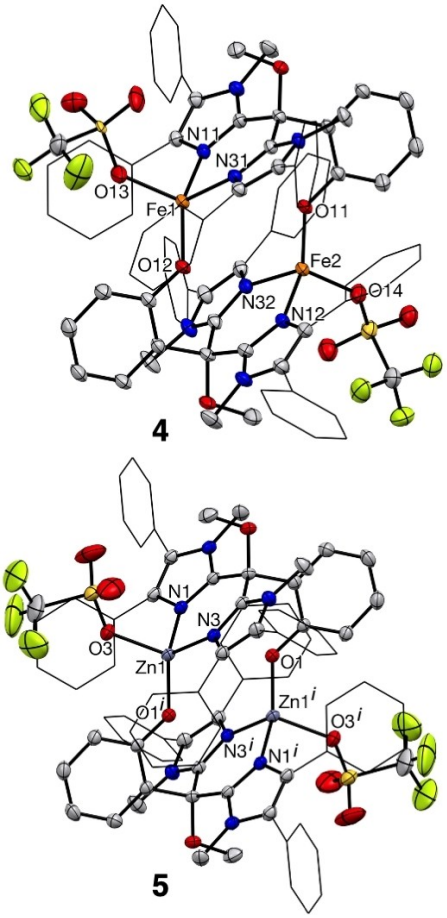

Figure 10. Displacement ellipsoid plots (50% probability level) for **4** and **5**. All H-atoms, disorder at the OTf groups and any co-crystallised solvent molecules have been omitted for clarity. Imidazole phenyl substituents are depicted in the wireframe format for clarity. Symmetry code *i*: 1-*x*, 1-*y*, 1-*z*.

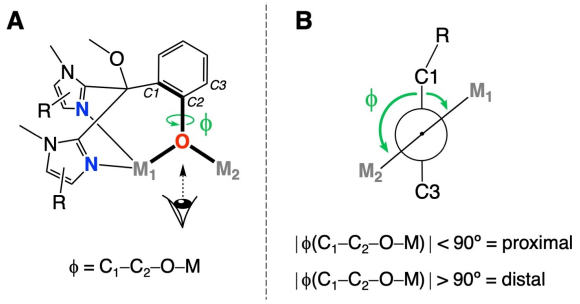

Figure 11. A: The C–C–O–M torsion angle (ϕ). B: Newman-type projection along the phenolate C–O bond, highlighting the C–C–O–M torsion angles associated to proximal or distal phenolate lone pair coordination.

triflate anion. The cyclic, dinuclear configuration of **4** and **5** means their metal centres can be regarded as occupying facially opposing sites,[33,34] with large intermetallic distances of 4.2589(6) Å and 3.9940(4) Å respectively. Selected bond lengths and bond angles are provided in Tables S3 and S4.

The X-ray crystal structures obtained for **4** and **5** are centrosymmetric. Selected bond lengths and bond angles are given in Table S3. The Fe1–O_{phen} bond length of 1.9061(12) Å and the Zn1–O_{phen} bond length of 1.8767(13) Å are similar to those previously reported for other four-coordinate iron and zinc centres bound to monodentate, anionic phenolic oxygen atoms. The Fe–N bond lengths in **4** (> 2 Å) are consistent with high-spin iron(II).[26,27]

Due to the ligand's bridging coordination mode, the triadic *N,N,O* donor set bound to each metal atom in **4** and **5** is not linked by a central quaternary carbon atom, as would be the case for a κ_3-*N,N,O* ligand. This has an influence on the tetrahedral distortion at each metal centre, exemplified by the large N–M–O_{phen} and O_{phen}–M–O_{OTf} angles that are all greater than 109.5°. For comparison, corresponding angles within mononuclear iron and zinc complexes supported by κ_3-*N,N,O* ligands are generally smaller than 100°.[8,26,27] The absence of the κ_3-type "cage" effect enables the metal ions in **4** and **5** to bind in an almost planar fashion with respect to the aromatic planes of the imidazole rings. Indeed, the Fe-N and Zn–N bond lengths in **4** and **5** are slightly shorter compared to those previously reported in our group for iron and zinc complexes bound to κ_3-*N,N,O* bis-imidazole-derived ligands.[26,27,30,31] We attribute this to better overlap of the imidazole lone pair with the in-plane metal *d*-orbitals, enabled by the bridging coordination of the **Im^{Ph2}NNO** ligand.

Finally, we observe C^{Ar}–C^{Ar}–O–M torsion angles (ϕ) of 176.59(12)° and −174.53(15)° in **4** and **5**, respectively, which indicates that the phenolate O-atoms coordinate exclusively through their distal lone pair to the second metal centre. Indeed, the C^{Ar}–C^{Ar}–O–M torsion angle is a useful parameter to determine which phenolate lone pair engages in metal coordination (Figure 11). Coordination of the proximal lone pair results in a $|\phi(C^{Ar}–C^{Ar}–O–M)|$ smaller than 90° (i.e. a *cis*-type orientation), and coordination of the distal lone pair results in a $|\phi(C^{Ar}–C^{Ar}–O–M)|$ greater than 90° (i.e. a *trans*-type orientation). The involvement of the phenolate's proximal or distal lone pair in metal coordination therefore appears to be dependent on the bulkiness of the ligand's constituent imidazole groups: **ImNNO** coordinates exclusively through its proximal lone pair,[30] whereas **BenzImNNO** can coordinate through both its proximal and distal lone pairs, and **Im^{Ph2}NNO** coordinates exclusively through its distal lone pair. The increased steric bulk of the imidazole also has the effect of reducing the coordination number of the metal centre, as evidenced by the 4-coordinate nature of the metal centres in **4** and **5** compared to the 6-coordinate metal centres in complexes supported by **ImNNO** or **BenzImNNO**.

Electronic structure and magnetism of 4

The dinuclear nature of **4** offers further intrigue with respect to its electronic structure and magnetism. The zero-field ^{57}Fe Mössbauer spectrum of **4** (Figure 12) exhibits a single quadrupole doublet, with an isomer shift (δ) of 1.02 mm s^{-1} and a quadrupole splitting ($|\Delta E_Q|$) of 3.26 mm s^{-1}. These parameters

Research Article
doi.org/10.1002/ejic.202101046

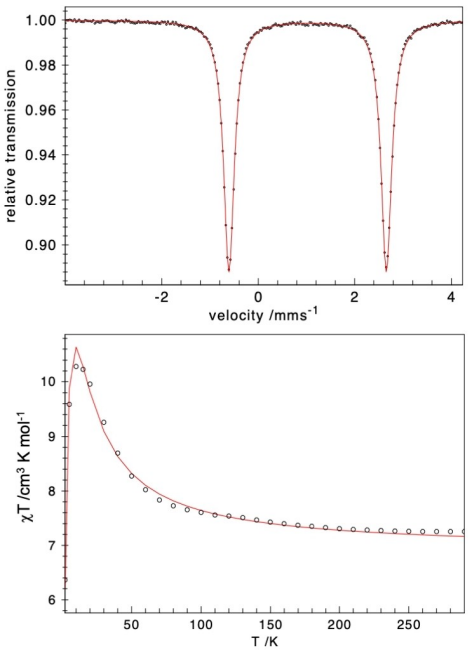

Figure 12. Top: The zero field ^{57}Fe Mössbauer spectrum of **4**, recorded at 80 K. The black points correspond to the experimental data and the red trace represents the best fit. Data fit parameters: $\delta = 1.02$ mm s^{-1}, $|\Delta E_Q| = 3.26$ mm s^{-1}. Bottom: temperature dependence of the magnetic moment of a powdered sample of **4**, measured by SQUID magnetometry. Black circles correspond to the experimental data and the red trace represents the best spin-Hamiltonian fit with $J = 1.9$ cm^{-1}, $D_{Fe} = 1.8$ cm^{-1}, $E_{Fe}/D_{Fe} = 0$, $g_{iso} = 2.145$.

are consistent with high-spin ($S = 2$) iron(II) and establish the equivalence of the two iron centres. SQUID magnetometry (Figure 12) reveals an χT value of approximately 7 cm^3 K mol^{-1} at room temperature, consistent with the presence of two uncoupled high-spin ($S = 2$) iron(II) centres. Upon cooling, the χT value gradually increases and reaches a maximum of approximately 10.5 cm^3 K mol^{-1} at 10 K. The experimental findings thus indicate that the ground state of **4** features weak ferromagnetic coupling of the two iron(II) centres and that their local spin states do not change even at low temperature. The simulations give an exchange coupling constant (J) of approximately 2 cm^{-1}. On this basis, we argue that the coupling energy is too weak to play a significant role during the reactivity of **4** at room temperature, as its effects would be negligible compared to the thermal excitations on the order of kT at 300 K. Therefore, complex **4** may be regarded as containing two electronically independent high-spin Fe(II) sites within its biomimetic framework.

Solution state behaviour of 4 and 5

Next, we investigated the solution state behaviour of **4** and **5** by NMR spectroscopy in order to establish whether the ligand's dinucleating μ_2:κ_2-*N,N,*:κ_1-*O* coordination mode is retained in solution. The ^{1}H NMR spectrum of **5** in THF-d_8 (Figure 13) shows a well-resolved set of ligand signals, the assignment of which was achieved through a combination of ^{1}H-^{1}H COSY and 1D TOCSY NMR experiments (Figures S71-S75). The spectrum contains two sharp singlets at 3.68 and 3.49 ppm, assigned to the N-methyl and O-methyl groups, respectively, on the basis of their 2:1 integral ratio. A single set of imidazole-derived aromatic signals is observed (resonances **E-J**), implying C_S ligand symmetry that is either consistent with the solid-state structure of **5** or, alternatively, could correspond to a mononuclear complex with κ_3-*N,N,O* ligand coordination.[26,28] The ^{19}F NMR spectra of **5** in THF-d_8 and MeCN-d_3 show a single, sharp resonance at −79 ppm, indicative of rapid exchange of the triflate anions with coordinating solvents.

We performed 1D NOE experiments in order to detect any long-range interactions that would only arise from a dinuclear structure in solution (Figure 13). Selective excitation of the resonances associated to the N-methyl group (**NMe**) and the H-atom *ortho* to the phenolate (**D**) produced NOE cross-peaks corresponding to **H** (the H-atoms on the *ortho* position of the imidazole 4-position phenyl ring). In the X-ray crystal structure of **5**, the **H**···**D** and **H**···**NMe** separations within the same ligand molecule (i.e. "*intra*-ligand") are measured as 6.81 Å and 5.46 Å, respectively, which surpass the generally accepted limit of 5 Å for NOE coherence transfer. In contrast, the **H**···**D** and **H**···**NMe**

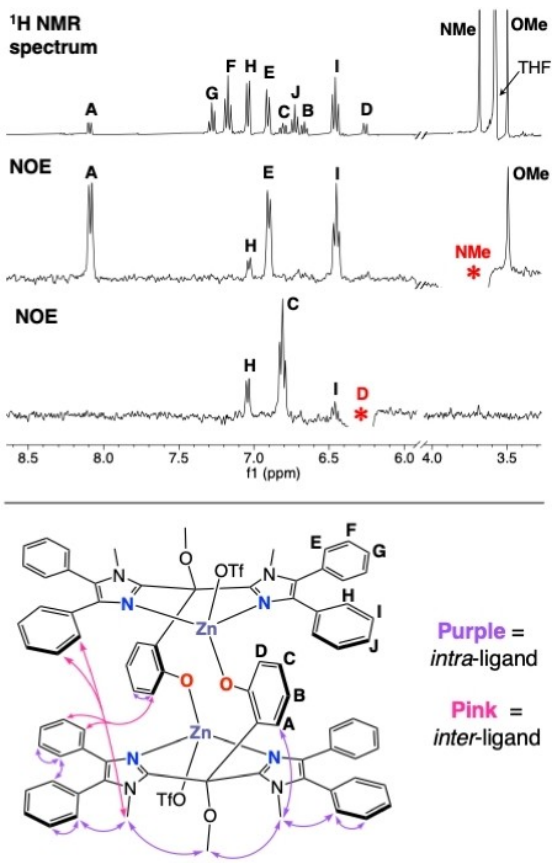

Figure 13. Top: ^{1}H NMR (400 Hz) spectrum of **5** and the NOESY spectra obtained for the selective excitation of resonances **D** and **NMe**, all recorded in THF-d_8 at 25 °C. Spectra are clipped for clarity. Bottom: Schematic depiction of the through-space NOE interactions detected by NOESY NMR analysis.

Research Article
doi.org/10.1002/ejic.202101046

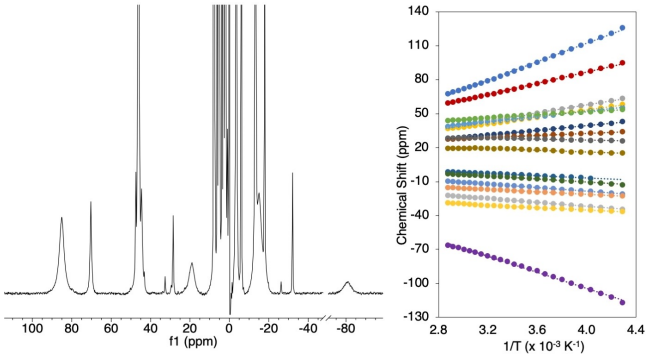

Figure 14. Left: The ^{1}H NMR spectrum of **4**, recorded in CD_3CN at 25 °C. Right: The inverse temperature dependence of the chemical shifts of **4**.

separations between the two different ligand molecules (i.e. "*inter*-ligand") are 3.58 Å and 3.72 Å, respectively. Thus, the fact that NOE cross-signals for H are detected upon selective excitation of **NMe** and **D** provide evidence that **5** retains its dinuclear structure in THF solution. Additionally, no temperature-dependent fluxional processes were observed upon conducting variable temperature (VT) NMR analysis of **5** in THF-d_8 (Figure S76) On this basis, we conclude that the dinuclear structure of **5** is stable across a large temperature range.

The ^{1}H NMR spectrum of **4** in MeCN-d_3 (Figure 14) contains highly paramagnetically shifted signals between 90 and −90 ppm, consistent with the presence of high-spin iron(II). Due to the large number of peaks as well as the severely broadened and overlapped nature of certain signals, assignment of the spectrum could not be made. The effective magnetic moment (μ_{eff}) of the complex was determined by Evans NMR method as being 6.49 μ_B at 25 °C, consistent with the presence of two high-spin ($S = 2$) ferrous ions.[33] The ^{19}F spectrum of **4** in MeCN-d_3 shows a single, sharp resonance at −79 ppm. VT ^{1}H NMR of **4** in MeCN-d_3 shows an increase in magnetization at low temperature that is consistent with normal Curie behaviour (Figure S60). The plot of signal shift (ppm) against 1/T (K^{-1}) produces linear fits for all peaks with convergence to the diamagnetic region upon extrapolation to infinite temperature. This demonstrates that no spin cross-over phenomena occur and supports the absence of any solvent-related coordination equilibria or structural changes. Based on this data, we propose that, analogously to its zinc counterpart, **4** has a dinuclear structure in solution that remains intact across a wide temperature range.

Dinuclear metal thiolate complexes

We were keen to investigate the substitutional lability of the triflate ligand in both **4** and **5** for biorelevant co-ligands and test the robustness of the ligand's dinucleating μ_2:κ_2-*N,N,*:κ_1-*O* coordination mode during substitution reactions. We employed thiophenolate for these investigations as a simple monodentate thiolate that is of structural relevance to the substrate-bound active site of isopenicillin N synthase (IPNS).[34] Analogous procedures were employed for the substitution reactions involving **4** and **5** (Scheme 6). The dinuclear triflate complex was dissolved in THF under inert conditions, after which NaSPh (2 equiv.) suspended in THF was added dropwise to the solution. After a period of approximately 5 min, a white, amorphous solid precipitated from the mixture. The suspension was stirred for a further 1.5 h before removal of all solvents under vacuum. The crude solid was subsequently extracted into dichloromethane solution, filtered, and dried under vacuum. The resulting dinuclear thiolate complexes $[Fe_2(Im^{Ph2}NNO)_2(SPh)_2]$ (**6**) and $[Zn_2(Im^{Ph2}NNO)_2(SPh)_2]$ (**7**) were obtained as white solids in yields of 78% and 71%, respectively. Single crystals suitable for X-ray diffraction were obtained by slow vapour diffusion of *n*-hexane into THF solutions of each complex under ambient conditions. The X-ray crystal structures are displayed in Figure 15, with selected bond lengths and bond angles provided in Tables S5 and S6.

The X-ray crystal structures show that **6** and **7** have retained a dinuclear, cyclic structure analogous to that of their triflate counterparts. In other words, substitution of the OTf ligands in **4** and **5** for one equivalent of SPh per metal ion was successful and did not cause any disruption of the supporting ligand's unique dinucleating μ_2:κ_2-*N,N*:κ_1-*O* coordination mode. Each metal centre has a distorted tetrahedral geometry, bound by the *N,N,O* donor set of the supporting ligand scaffold and the anionic sulfur atom of a thiophenolate co-ligand. Notwithstanding the dinuclear nature of **6** and **7**, the independent metal sites in these complexes can be regarded as structural models of the substrate-bound active site of IPNS.[36]

The X-ray crystal structures of **6** and **7** are centrosymmetric. As was the case for their triflate counterparts, large C–O–O–M torsion angles are observed in both complexes (−179.07(17)° and 176.60(16)° for **6** and **7**, respectively), consistent with the coordination of the phenolic oxygen atom through its distal lone pair. Similarly, the metal centres are bound in an almost co-planar fashion with respect to the bis-imidazole methane moiety of the ligand scaffold. The tetrahedral distortion at each metal centre is manifested by the N–M–O and S–M–O angles that are all larger than that of an ideal tetrahedron. The M–S–C

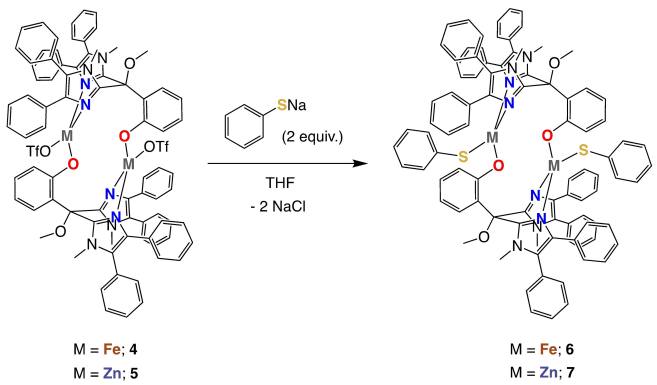

Scheme 6. Synthesis of dinuclear complexes $[Fe_2(Im^{Ph2}NNO)_2(SPh)_2]$ (**6**) and $[Zn_2(Im^{Ph2}NNO)_2(SPh)_2]$ (**7**).

Research Article
doi.org/10.1002/ejic.202101046

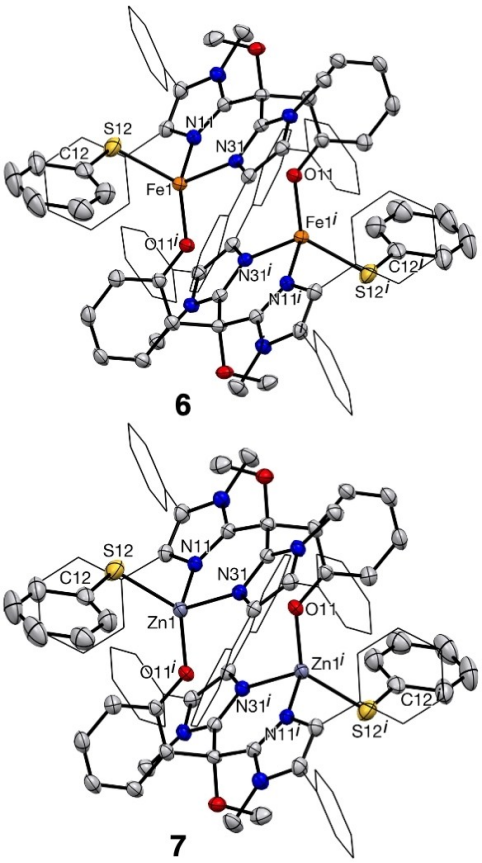

Figure 15. Displacement ellipsoid plots (50% probability level) for **6** (left) and **7** (right). All hydrogen atoms and disorder at the phenyl substituents have been omitted for clarity. Imidazole phenyl substituents are depicted in the wireframe format for clarity. Symmetry code *i*: 1-*x*, 1-*y*, 1-*z*.

bond angles of 115.20(11)° and 114.41(9)° for **6** and **7**, respectively, are consistent with the sp^3 hybridisation and tetrahedral geometry of the thiolate sulfur atoms. The angles, however, are somewhat larger compared to those reported for other metal thiophenolate complexes supported by a tripodal *N,N,O* ligand.[14,31,37] We attribute this to the relatively close proximity of the thiophenolate and phenolate rings. The M-S bond distances of 2.3245(9) Å and 2.2870(9) Å for **6** and **7**, respectively, are in line with those of other previously reported iron(II) and zinc(II) complexes with monodentate thiolate ligands.[14,31,38,39] The intermetallic distances of 4.4996(6) Å and 4.5072(6) Å in **6** and **7**, respectively, are almost identical and represent an increase of 0.2407(8) Å and 0.5132(7) Å relative to their respective parent triflate complexes. These changes can be rationalised using Bent's rule[40] and by examining the changes in hybridization taking place within the metal-ligand bonds (further discussion in the supporting information).

The zero-field ^{57}Fe Mössbauer spectrum of **6** (Figure S83) shows a single quadrupole doublet, best described by an isomer shift of 0.96 mm s^{-1} and a quadrupole splitting of 3.07 mm s^{-1}. The Mössbauer lines are unusually broad and a slight asymmetry in the quadrupole doublet is observed, which we attribute to a distribution of quadrupole splittings that may arise from some slight(micro)heterogeneity in the powder sample of **6**.[41] This likely causes some inequivalence of the dimers within the powder macrostructure rather than the inequivalence of the two iron sites within the dinuclear complex. Low crystallinity and high surface effects of an amorphous powder sample have typically been invoked as origin effects for this phenomenon. Overall, the Mössbauer spectrum obtained for **6** is consistent with the presence of two electronically equivalent high-spin iron(II) centres. Finally, we observe that the isomer shift for complex **6** is slightly lower compared to that of **4**. This is due to the substitution of the hard oxygen-rich triflates for soft sulfur atoms of the thiophenolate ligands, whose stronger covalent interactions cause more s-electron density to be donated to the iron centre, giving rise to a more negative isomer shift.

DFT calculations

We performed density functional theory (DFT) calculations in order to investigate the influence of the thiophenolate ligands on the electronic properties of the dinuclear complexes. The gas-phase geometries of complexes **4**-**7** were optimised at the B3LYP/6-311 g(d,p) level of theory. The Kohn-Sham molecular orbitals (MOs) were extracted from these geometries for zinc complexes **5** and **7**. For iron complexes **4** and **6**, the α and β MOs were biorthogonalised using the *Multiwfn* program,[42] and their energies evaluated using the Fock matrix generated by natural bonding orbital (NBO) analysis. The highest occupied molecular orbitals (HOMO) calculated for each complex are depicted in Figure 16.

The HOMO in **5** is delocalised across both phenolic moieties of the supporting ligand molecules, which demonstrates their

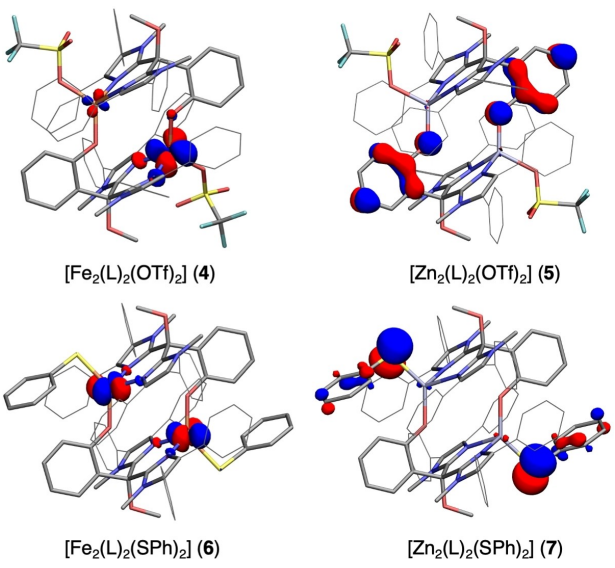

Figure 16. The HOMOs of the OTf dimers (**4** and **5**) and the SPh dimers (**6** and **7**) as calculated by DFT at the B3LYP/6-31 g(d,p) level of theory. Isosurfaces are drawn at ±0.05. Imidazole phenyl substituents have been depicted in the wireframe format for clarity.

redox non-innocent character. However, substitution of the OTf groups for SPh ligands in **7** shifts the HOMO to the lone pairs of the sulfur atoms. We attribute the greater oxidation susceptibility of the thiophenolate ligands to the lower ionisation potential of sulfur in general. In contrast, the eight highest occupied molecular orbitals in **4** and **6** are all singly occupied iron-based orbitals, in line with the spin density being localised entirely on the iron centres (Figure S103). Thus, theory predicts that the iron centres in both **4** and **6** are the sites most prone to oxidation despite the presence of redox active phenolate or thiophenolate moieties within the same complex architecture. Interestingly, computations show that the HOMO in **4** takes its greatest contribution from a d-orbital localised on one of the iron centres, whereas the HOMO in **6** takes an equal contribution from two d-orbitals, one per iron centre. This could be due to the very slight ferromagnetic magnetic coupling observed between the iron centres in **4** compared to **6**, where it is likely that no magnetic coupling occurs at all. The Fe···Fe distances observed in the X-ray crystal structures of **4** and **6** are 4.2589(6) Å and 4.4996(6) Å, respectively.

Reactivity of 6

Complex $[Fe_2(Im^{Ph2}NNO)_2(SPh)_2]$ (**6**) is of structural relevance to the substrate-bound active site of isopenicillin N synthase as it contains independent iron(II) centres, each capped by a supporting *N,N,O* ligand and bound to an exogenous thiolate. It is therefore of interest to investigate the site at which oxidation occurs when exposing the complex to different oxidants. DFT calculations predict that the iron centres are the sites most prone to oxidation. However, the thiolate sulfur atoms, situated at the apical sites of the complex, are relatively "exposed" and could easily be targeted by oxidants in solution.

Reacting **6** with PhIO (10 equiv.) in MeCN at room temperature induces a slow colour change from orange to deep red, which is manifested by the development of a UV-vis absorption band at 475 nm that shoulders the intense π-π* transition region of the spectrum (Figure 17). Analysis of the resulting solution by means of ESI-MS in negative mode shows a signal at *m/z* = 156.90, which corresponds to the phenylsulfonate anion (calculated *m/z* = 157.00 for $PhSO_3^-$). In positive mode ESI-MS, a strong signal is detected at *m/z* = 601.1, which corresponds to the free ligand. An additional much weaker signal was observed at *m/z* = 571.1, which corresponds to the methoxy-cleaved ligand (calculated *m/z* = 571.25 for $[L{-}OCH_3]^-$), and is likely the result of oxidative ligand degradation to its quinone form. No iron-containing ions could be detected, most probably due to hydrolysis of the complexes under the ESI-MS measurement conditions. For comparison, we monitored the oxidation of **6** in air by UV-vis spectroscopy and observed the development of the same absorption band at 475 nm (Figure 17). We do not observe any absorption band at 580 nm, as had been the case for the oxidation of $[Fe_2(Im^{Ph2}NNO)_2(OTf)_2]$ (**4**) in air. On this basis, we tentatively assign the band at 475 nm to an iron(III) sulfonate complex, which may derive from a short-lived iron-oxo intermediate that is not observed by UV-vis.

Unexpected C–O bond cleavage in the presence of $FeCl_3$

Reacting **K-Im^{Ph2}NNO** with one equivalent of $FeCl_3$ in MeCN resulted in the immediate formation of a deep blue solution. The solution was stirred for a further 1.5 h before being filtering and dried under vacuum, affording a dark blue solid. The UV-vis spectrum of this species in CH_2Cl_2 exhibits a broad absorption band at 612 nm (Figure 18). Interestingly, we observed that the sample solution progressively changed colour from blue to red, coupled to a shift in the absorption band to 470 nm. A similar phenomenon was observed when dissolving the blue solid in THF: the solution was initially blue but swiftly changed colour to red. In UV-vis spectroscopy, we observe a shift in the absorption band from 590 to 470 nm. The spectrum recorded when the THF solution was visibly still blue is severely broadened due to a contribution from the band rapidly forming at 470 nm.

Red crystals suitable for X-ray diffraction were obtained by slow diffusion of *n*-hexane into a THF solution of the reaction product over the course of several days. The resulting X-ray

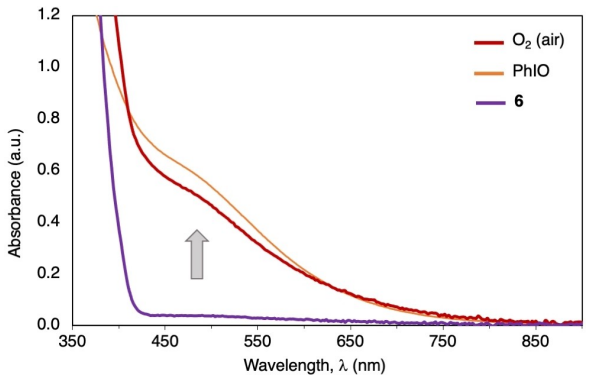

Figure 17. Overlay of the UV-vis spectra obtained after reacting **6** with PhIO (10 eq.) or O_2 (air).

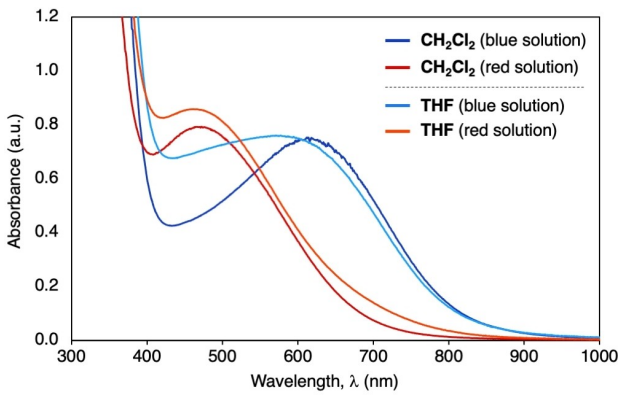

Figure 18. UV-vis spectra of the blue and red solutions of the product obtained from the reaction of **K-Im^{Ph2}NNO** and $FeCl_3$. Spectra were recorded at ambient temperature for CH_2Cl_2 and THF solutions of the product.

Research Article
doi.org/10.1002/ejic.202101046

crystal structure reveals the formation of a diiron(III) complex, $[Fe_2(Im^{Ph2}NNO^*)_2(Cl)_2]$ (**8**), featuring two ligand molecules ($Im^{Ph2}NNO^*$) that have undergone methyl cleavage (C–O bond cleavage) at the methoxy group (Figure 19). The iron nuclei are bound within a diamond core structure, with an intermetallic distance of 3.0830(8) Å. Each iron centre is pentacoordinate and square pyramidal in geometry, bound to the imidazole group of one ligand molecule, the phenolate group of a second ligand molecule, a chloride ion and two anionic μ_2-bridging alkoxide oxygen atoms from the degraded ligand molecules. One imidazole group in both ligand molecules remains non-coordinated. Selected bond lengths and bonds angles are given in Table S7.

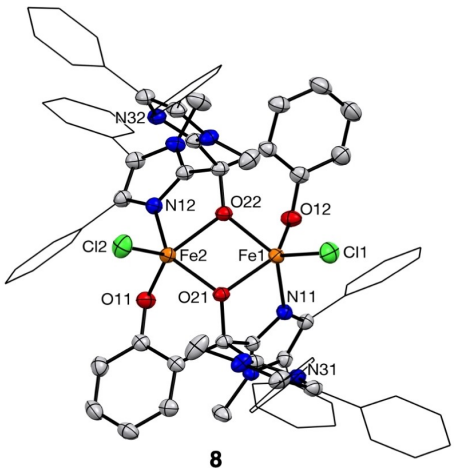

Figure 19. Displacement ellipsoid plot of $[Fe_2(Im^{Ph2}NNO^*)(Cl)_2]$ (**8**), drawn at the 50% probability level. All hydrogen atoms are omitted for clarity. Imidazole Ph substituents are drawn in the wireframe format for clarity.

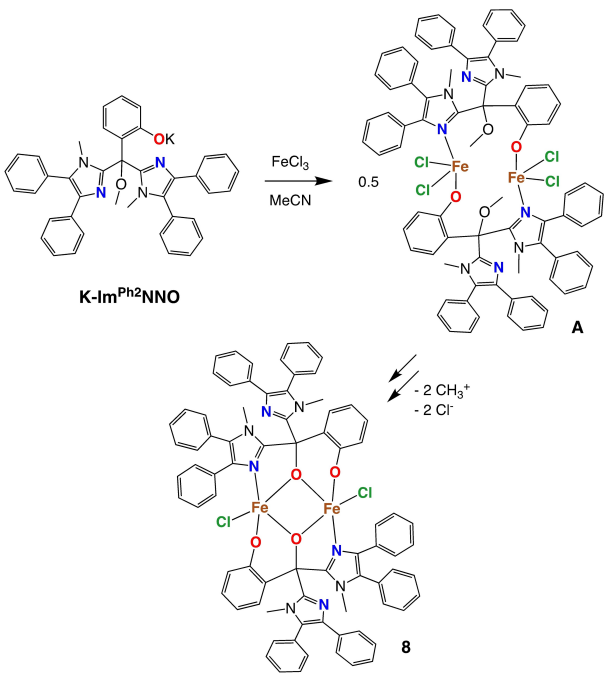

Scheme 7. The reaction between **K-Im^{Ph2}NNO** and $FeCl_3$ leading to the formation of complex **8** *via* the proposed intermediate **A**.

The degradation of the ligand in this manner is somewhat unexpected given the poor leaving group ability generally associated to methyl groups. However, demethylation of protected hydroxyl groups through C–O bond cleavage has been reported in the presence of strong Lewis acids such as BBr_3,[43,44] $AlCl_3$,[45] and $FeCl_3$.[46,47] We hypothesise that reaction of **K-Im^{Ph2}NNO** with $FeCl_3$ initially produces a blue-coloured intermediate diiron(III) complex, $[Fe_2(Im^{Ph2}NNO)_2(Cl)_4]$ (**A**), which contains two ferric ions within the dinuclear, cyclic complex architecture associated to the ligand's μ_2-coordination mode (Scheme 7). However, the strong metal-halide interaction combined with the steric congestion associated to the presence of two chloride ions in the iron's coordination sphere likely causes one of the imidazole groups to dissociate, which has the effect of bringing the methoxy groups into closer proximity to the metal centres,[31] and enables the red-coloured complex **8** to form through C–O bond cleavage. We also propose that the leaving group ability of the alkylate is enhanced by the coordination of the resulting anionic alkoxide oxygen atoms to the Fe^{3+} ions.

Conclusions

We have synthesised two new bis-imidazole-derived phenolate ligands, **BenzImNNO** and **Im^{Ph2}NNO**, which feature 1-methlbenzimidazole and 1-methyl-4,5-diphenylimidazole groups, respectively. These new ligands expand the library of bioinspired *N,N,O* ligands designed to structurally model the 2-His-1-Carboxylate facial triad (2H1C). We have shown that **BenzImNNO** readily coordinates by means of a facial κ_3-*N,N,O* binding motif. However, the 1-methylbenzimidazole groups are small enough for homoleptic, bisligated complexes to form in reactions involving either one or two equivalents of ZnX_2 salt (X = Cl or OTf). In these complexes, the phenolic oxygen atoms have the propensity to adopt a μ_2-bridging coordination mode to a second metal centre, giving rise to dinuclear complexes of the type $[Zn(BenzImNNO)_2Zn(X)_2]$. The Zn_2O_2 diamond core structure in these complexes involves the coordination of both the proximal and distal lone pairs of the phenolic oxygen atoms. In contrast, the 1-methyl-4,5-diphenylimidazole groups in **Im^{Ph2}NNO** are too sterically cumbersome to enable homoleptic, bisligated complexes to form. Instead, reacting the ligand with one equivalent of $M(OTf)_2$ (M = Fe or Zn) produces dinuclear complexes of the type $[M_2(Im^{Ph2}NNO)_2(OTf)_2]$, where the ligand adopts a unique μ_2:κ_2-*N,N*:κ_1-*O* coordination mode that locks the two metals within a large 14-membered ring structure. The phenolic oxygen atoms in these complexes coordinate exclusively through their distal lone pairs. The two metal ions are separated by a large intermetallic distance and can be regarded as electronically and magnetically independent entities. In the case of iron, this is confirmed by Mössbauer spectroscopy and SQUID magnetometry. We have furthermore shown that the apical triflate ligands can be substituted for thiophenolate ligands, generating dinuclear thiolate complexes

of the type $[M_2(Im^{Ph2}NNO)_2(SPh)_2]$. These complexes are of structural relevance to the substrate-bound active site of IPNS. Reacting $[Fe_2(Im^{Ph2}NNO)_2(SPh)_2]$ (complex **6**) with either O_2 or PhIO produces a new red-coloured species in solution that we assign as an iron(III) sulfonate species on the basis of UV-vis and ESI-MS studies. However, reacting **Im^{Ph2}NNO** with Lewis acidic $FeCl_3$ leads to the unexpected methyl cleavage of the ligand's methoxy group. These observations point out that more complex structural and chemical transformations take place upon oxidation of the iron centres in **6**, which are currently under further investigation in our laboratories.

Overall, these results demonstrate that subtle steric differences between ligands of the same family can have a drastic impact on the structure of their related metal complexes. However, it is also evident that additional ligand design considerations beyond imidazole steric bulk are necessary in order to achieve the desired monoligated *N,N,O*-bound complex architecture that truly models the 2H1C. Indeed, it is likely that inclusion of a sterically bulky group *ortho* to the phenolate group is necessary to block its coordination through the distal lone pair and prevent any bridging coordination modes from occurring.

Experimental Section

All experimental details are provided in the supporting information.

Deposition Numbers 2126569 (for **H-Im^{Ph2}NNO**), 2126570 (for **3**), 2126571 (for **4**), 2126572 (for **5**), 2126573 (for **6**), 2126574 (for **7**), and 2126575 (for **8**) contain the supplementary crystallographic data for this paper. These data are provided free of charge by the joint Cambridge Crystallographic Data Centre and Fachinformationszentrum Karlsruhe Access Structures service www.ccdc.cam.ac.uk/structures.

Acknowledgements

This work was financially supported by the European Union under the Marie Sklodowska-Curie NoNoMeCat ITN network grant agreement (675020-MSCA-ITN-2015-ETN). The X-ray diffractometer was financed by the Netherlands Organisation for Scientific Research (NWO). This work was sponsored by NWO Exacte en Natuurwetenschappen (Physical Sciences) for the use of supercomputer facilities. We also wish to thank Bernd Mienert and Andreas Göbels (MPI) for their technical assistance with the Mössbauer and SQUID measurements. We kindly thank our colleagues Dr. Johann Jastrzebski, Dr. Léon Witteman and Serhii Tretiakov at Utrecht University for their assistance and helpful discussions regarding the NMR experiments.

Conflict of Interest

The authors declare no conflict of interest.

Data Availability Statement

The data that support the findings of this study are available from the corresponding author upon reasonable request.

Keywords: Bioinorganic chemistry · Enzyme models · IPNS · Iron · *N,N,O* ligands

[1] K. D. Koehntop, J. P. Emerson, L. Que Jr., *J. Biol. Inorg. Chem.* **2005**, *10*, 87–93.
[2] L. Que Jr., *Nat. Struct. Biol.* **2000**, *7*, 182–184.
[3] L. Que Jr., W. B. Tolman, *Nature* **2008**, *455*, 333–340.
[4] H. Park, D. Lee, *Chem. A Eur. J.* **2020**, *26*, 1–12.
[5] P. C. A. Bruijnincx, G. van Koten, R. J. M. Klein Gebbink, *Chem. Soc. Rev.* **2008**, *37*, 2716.
[6] L. Vicens, G. Olivo, M. Costas, *ACS Catal.* **2020**, *10*, 8611–8631.
[7] M. Costas, M. P. Mehn, M. P. Jensen, L. Que Jr., *Chem. Rev.* **2004**, *104*, 939–986.
[8] A. Beck, B. Weibert, N. Burzlaff, *Eur. J. Inorg. Chem.* **2001**, 521–527.
[9] A. Beck, A. Barth, E. Hübner, N. Burzlaff, *Inorg. Chem.* **2003**, *42*, 7182–7188.
[10] I. Hegelmann, A. Beck, C. Eichhorn, B. Weibert, N. Burzlaff, *Eur. J. Inorg. Chem.* **2003**, 339–347.
[11] N. Burzlaff, *Tripodal N,N,O-Ligands for Metalloenzyme Models and Organometallics*, R. van Eldik, Ed.; Elsevier, Vol. 60, **2008**, pp.
[12] T. C. Higgs, C. J. Carrano, *Inorg. Chem.* **1997**, *36*, 298–306.
[13] B. S. Hammes, C. J. Carrano, *Inorg. Chem.* **1999**, *38*, 3562–3568.
[14] J. N. Smith, Z. Shirin, C. J. Carrano, *J. Am. Chem. Soc.* **2003**, *125*, 868–869.
[15] P. J. Cappillino, J. R. Miecznikowski, L. A. Tyler, P. C. Tarves, J. S. McNally, W. Lo, B. S. T. Kasibhatla, M. D. Krzyaniak, J. McCracken, F. Wang, W. H. Armstrong, J. P. Caradonna, *Dalton Trans.* **2012**, *41*, 5662.
[16] J. McCracken, P. J. Cappillino, J. S. McNally, M. D. Krzyaniak, M. Howart, P. C. Tarves, J. P. Caradonna, *Inorg. Chem.* **2015**, *54*, 6486–6497.
[17] P. D. Oldenburg, A. A. Shteinman, L. Que Jr., *J. Am. Chem. Soc.* **2005**, *127*, 15672–15673.
[18] P. D. Oldenburg, C.-Y. Ke, A. A. Tipton, A. A. Shteinman, L. Que Jr., *Angew. Chem. Int. Ed.* **2006**, *45*, 7975–7978; *Angew. Chem.* **2006**, *118*, 8143–8146.
[19] S. Paria, P. Halder, T. K. Paine, *Inorg. Chem.* **2010**, *49*, 4518–4523.
[20] V. J. Dungan, S. M. Wong, S. M. Barry, P. J. Rutledge, *Tetrahedron* **2012**, 3231–3236.
[21] K. Valegård, A. C. T. van Scheltinga, M. D. Lloyd, T. Hara, S. Ramaswamy, A. Perrakis, A. Thompson, H.-J. Lee, J. E. Baldwin, C. J. Schofield, J. Hajdu, I. Andersson, *Nature* **1998**, 394, 805–809.
[22] P. C. A. Bruijnincx, M. Lutz, A. L. Spek, E. E. van Faassen, B. M. Weckhuysen, G. van Koten, R. J. M. Klein Gebbink, *Eur. J. Inorg. Chem.* **2005**, *4*, 779–787.
[23] P. C. A. Bruijnincx, M. Lutz, J. P. den Breejen, A. L. Spek, G. van Koten, R. J. M. Klein Gebbink, *JBIC J. Biol. Inorg. Chem.* **2007**, *12*, 1181–1196.
[24] P. C. A. Bruijnincx, I. L. C. Buurmans, S. Gosiewska, M. A. H. Moelands, M. Lutz, A. L. Spek, G. van Koten, R. J. M. Klein Gebbink, *Chem. A Eur. J.* **2008**, *14*, 1228–1237.
[25] P. C. A. Bruijnincx, M. Lutz, A. L. Spek, W. R. Hagen, B. M. Weckhuysen, G. van Koten, R. J. M. Klein Gebbink, *J. Am. Chem. Soc.* **2007**, *129*, 2275–2286.
[26] M. A. H. Moelands, S. Nijsse, E. Folkertsma, B. de Bruin, M. Lutz, A. L. Spek, R. J. M. Klein Gebbink, *Inorg. Chem.* **2013**, *52*, 7394–7410.
[27] E. Folkertsma, E. F. de Waard, G. Korpershoek, A. J. van Schaik, N. Solozabal Mirón, M. Borrmann, S. Nijsse, M. A. H. Moelands, M. Lutz, M. Otte, M.-E. Moret, R. J. M. Klein Gebbink, *Eur. J. Inorg. Chem.* **2016**, *9*, 1319–1332.
[28] E. C. Monkcom, P. Ghosh, E. Folkertsma, H. A. Negenman, M. Lutz, R. J. M. Klein Gebbink, *Chim. Int. J. Chem.* **2020**, *74*, 450–466.
[29] J. Fernández-Baeza, A. Antiñolo, J. Tejeda, A. Lara-Sánchez, A. Otero, *Dalton Trans.* **2004**, 1499–1510.
[30] P. C. A. Bruijnincx, M. Lutz, A. L. Spek, W. R. Hagen, G. van Koten, R. J. M. Klein Gebbink, *Inorg. Chem.* **2007**, *46*, 8391–8402.
[31] E. C. Monkcom, D. de Bruin, A. J. de Vries, M. Lutz, S. Ye, R. J. M. Klein Gebbink, *Chem. A Eur. J.* **2021**, *27*, 5191–5204.
[32] D. L. Jameson, S. E. Hilgen, C. E. Hummel, S. L. Pichla, *Tetrahedron Lett.* **1989**, *30*, 1609–1612.

[33] S. Lindsay, S. K. Lo, O. R. Maguire, E. Bill, M. R. Probert, S. Sproules, C. R. Hess, *Inorg. Chem.* **2013**, *52*, 898–909.
[34] S. Lindsay, S. L. Mader, V. R. I. Kaila, C. R. Hess, *ChemistrySelect* **2018**, *3*, 1602–1608.
[35] B. Weber, E. Kaps, *Heteroat. Chem.* **2005**, *16*, 391–397.
[36] P. L. Roach, I. J. Clifton, C. M. H. Hensgens, N. Shibata, C. J. Schofield, J. Hajdu, J. E. Baldwin, *Nature* **1997**, *387*, 827–830.
[37] B. S. Hammes, C. J. Carrano, *Inorg. Chem.* **1999**, *38*, 4593–4600.
[38] Y. Zang, L. Que Jr., *Inorg. Chem.* **1995**, *34*, 1030–1035.
[39] K. P. Chiang, P. M. Barrett, J. M. Smith, S. Kingsley, W. W. Brennessel, M. M. Clark, R. J. Lachicotte, P. L. Holland, *Inorg. Chem.* **2009**, *48*, 5106–5116.
[40] H. A. Bent, *J. Chem. Educ.* **1960**, *37*, 616.
[41] M. Hans, W. Buckel, E. Bill, *JBIC J. Biol. Inorg. Chem.* **2008**, *13*, 563–574.
[42] T. Lu, F. Chen, *J. Comput. Chem.* **2012**, *33*, 580–592.
[43] P. A. Grieco, M. Nishizawa, T. Oguri, S. D. Burke, N. Marinovic, *J. Am. Chem. Soc.* **1977**, *99*, 5773–5780.
[44] M. Demuynck, P. De Clercq, M. Vandewalle, *J. Org. Chem.* **1979**, *44*, 4863–4866.
[45] S. M. Baars, J. O. Hoberg, *Carbohydr. Res.* **2006**, *341*, 1680–1684.
[46] B. Ganem, V. R. Small, *J. Org. Chem.* **1974**, *39*, 3728–3730.
[47] Y. Sawama, M. Masuda, S. Asai, R. Goto, S. Nagata, S. Nishimura, Y. Monguchi, H. Sajiki, *Org. Lett.* **2015**, *17*, 434–437.

Manuscript received: December 7, 2021
Revised manuscript received: February 4, 2022
Accepted manuscript online: February 6, 2022